

IMAGING OF OBJECTS THROUGH LOSSY LAYER WITH DEFECTS

X. X. Cheng, B.-I. Wu, H. Chen[†], and J. A. Kong[‡]

The Electromagnetics Academy at Zhejiang University
Zhejiang University
Hangzhou 310058, China

Abstract—The imaging method when a lossy layer (e.g., a defected metallic slab or a plasma layer) is present between the target and the sensor is demonstrated using the concept of active left-handed material (LHM). The effect of the lossy layer to the reflection coefficients measured by the receiver can be cancelled by imaginatively adding an active LHM layer, which has a same thickness as the lossy layer but an opposite sign of the constitutive parameters. Therefore, the updated reflection coefficients obtained after this data process look like the lossy layer has been removed, which leads to a significant improvement of the target imaging. When the lossy layer is inhomogeneous due to the existence of small defects, we use a homogenization procedure based on the Drude model to characterize its effective constitutive parameters. Our simulation examples shows the effectiveness of the proposed method.

1. INTRODUCTION

Using microwave signals to “see” through obstacles such as walls, doors, and other visually opaque materials is always an interesting and challenging topic [1–5], which offers powerful tools for a variety of applications in both military and commercial paradigms, such as rescue radar operation [1, 2], underground detection [4], Surveillance/navigation [5], etc. Through-the-wall imaging can tell what is happening or locate persons/assets on the other side of a wall, behind bushes, in the dark, in a tunnel or a cave, or through a dense fog.

[†] Author to whom correspondence should be addressed; electronic mail: chenhs@ewt.mit.edu

[‡] All authors also with Research Laboratory of Electronics, Massachusetts Institute of Technology, Cambridge, MA 02139, USA

It is seen that most “walls” are fairly transparent to radar frequencies, making the imaging through the wall to be possible. The material of the wall is very important to image quality. Usually they are limited to thin non-absorbing and non-metallic material in order to achieve a good image quality [1, 2]. When the obstacle becomes extraordinarily absorbing and lossy, or even possesses metallic-like property, it becomes increasingly difficult to see the target behind the “wall”.

In this present paper, we proposed a method to find the tiny target information from the raw measured data that recorded by the receiver. The case we investigated is that the object is behind a wall with large losses. The method utilizes the concept of left-handed material (LHM), which has simultaneously negative permittivity and permeability over a certain range of frequencies and thus can act as a phase compensator/conjugator. LHM has not only been plentifully realized and experimentally confirmed [6, 7] but also has opened many new possibilities in different applications [8–13]. In this method, an active LHM layer with the same thickness as the lossy obstacle layer is imaginatively inserted. The constitutive parameters (including both the real and imaginary parts) of the LHMs are exactly opposite to those of the lossy obstacle layer. Since the LHM layer can compensate the path where the electromagnetic wave goes through the obstacle layer, the effect of the lossy obstacle layer to the reflection coefficients measured by the receiver can be cancelled. Therefore, the retrieved reflection coefficients of the object looks like the lossy obstacle layer has been removed, leading to significant improvement of the object imaging.

In general, the proposed imaging procedure can be described as follows: Firstly, we need to know the information of the lossy layer (or lossy “wall”) including the thickness and the material property (permittivity and permeability). These information actually can be obtained in reality beforehand, for example, when we want to detect whether there are any cars or trucks below a forest, we can get the effective parameters of the forest beforehand. If the lossy layer is inhomogeneous, we also need to obtain its effective electromagnetic parameters by using a homogenization procedure. Secondly, by supposititiously adding an active LHM layer, we reconstruct the reflection coefficient without the effect of the lossy layer. Finally, the information of the target can be obtained by using the reconstructed reflection coefficient. The main challenge in this method is that in the real world the lossy layer is usually not homogeneous. There may be all sorts of defects in it, which is equivalent to the case that the raw data measured by the receiver contains noise. However, in most of the cases, the sizes of the defects, for example, narrow and short

slots, bubbles with small radius, tiny cracks, and so on, are usually very small compared with the operating wavelength. Therefore, it is possible to homogenize them with effective constitutive parameters.

The paper is organized as follows: In Section 2 we give a detailed description of the methodology on how we reconstruct the reflection coefficient of the target. Transmission line theory (TLT) is applied for one-dimensional (1-D) imaging. In Section 3, two typical kinds of defects are investigated and the suitable homogenization models are presented. In Section 4, we apply the methodology to reconstruct the reflected information of the target through different type of defects. We show significant improvement of the imaging quality can be achieved.

2. METHODOLOGY

We investigate a specific one-dimensional (1-D) case, in which the obstacle (lossy “wall”) might be plasma medium or thin metal. Without loss of generality, the frequency band is set to be 0~600 GHz, with the center frequency $f_c = 300$ GHz corresponding to a wavelength of $\lambda_c = 1$ mm. The thickness of the lossy “wall” is 0.1 mm ($\lambda_c/10$).

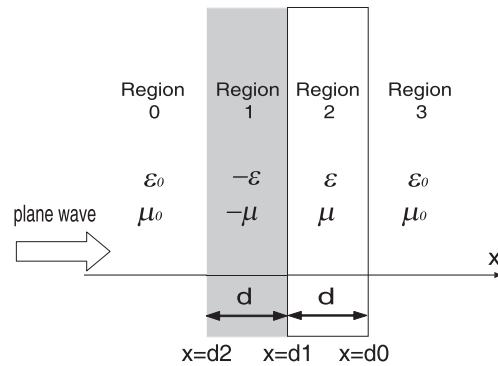


Figure 1. Transmission line theory for 1-D layered medium.

We use the transmission line theory to study the 1-D imaging problem. The well-known transmission line theory [14] is an efficient tool to solve the 1-D problem. As shown in Fig. 1, two layers are arranged along the wave propagating direction which is normal to the layers surfaces. According to the TLT, the ratio of E and H (input impedance) at any position only depends on the material parameters behind. Hence, we can treat the entire thing behind the layer that we are interested as a black box. For example, we treat Region 3 ($x > d_0$) in Fig. 1 as a black box, then we can obtain E and H fields at d_1

surface from the E and H field at d_0 surface by,

$$\begin{bmatrix} E(d_1) \\ H(d_1) \end{bmatrix} = \begin{bmatrix} \cos(kd) & -iZ \sin(kd) \\ -iY \sin(kd) & \cos(kd) \end{bmatrix} \begin{bmatrix} E(d_0) \\ H(d_0) \end{bmatrix} \quad (1)$$

where $k = \omega\sqrt{\epsilon\mu}$ is the wave vector, $Z = \sqrt{\mu/\epsilon}$ (for TE wave) is the characteristic impedance, $Y = 1/Z$, and d is the thickness of the layer inside Region 2 ($d_1 < x < d_0$). After that the generalized impedance and reflection coefficient at d_1 surface can both be calculated.

Similarly, if Region 1 (marked in gray in Fig. 1) is an LHM layer, Eq. (1) becomes the following form:

$$\begin{bmatrix} E(d_2) \\ H(d_2) \end{bmatrix} = \begin{bmatrix} \cos(kd) & iZ \sin(kd) \\ iY \sin(kd) & \cos(kd) \end{bmatrix} \begin{bmatrix} E(d_1) \\ H(d_1) \end{bmatrix} \quad (2)$$

where k has the same wave number, and d is also the thickness of Region 1 ($d_2 < x < d_1$). The matrix in Eq. (2) is in fact the inverse matrix of the one in Eq. (1), we call it inverted matrix in this paper, then we get exactly the identical field at d_2 surface as at d_0 surface, meaning $E(d_0) = E(d_2)$, $H(d_0) = H(d_2)$.

Furthermore, our idea of reconstructing the reflection coefficient without obstacle is illustrated in Fig. 1. In the real imaging, what we can get is usually the reflection coefficient at d_1 surface, where Region 2 ($d_1 < x < d_0$) is the really existent obstacle, but Region 1 ($d_2 < x < d_1$) is added imaginarily. The purpose of inserting one more layer is to cancel the effect of the obstacle slab (Region 2) and make it seems to disappear in the light of electromagnetic waves. Therefore, the supposititious layer (Region 1) should be an active LHM layer with exactly opposite signs of permittivity and permeability (including both real part and imaginary part) of Region 2 and with the same thickness as Region 2. In this way, Region 1 and Region 2 as a whole disappears when viewed externally; it is like this volume of space ($d_2 < x < d_0$) is stolen and the two interface of $x = d_0$ and $x = d_2$ overlap, which means the two surfaces have identical electrical and magnetic fields. Once we know the electric and magnetic fields at $x = d_0$, we can get the reflection coefficient at $x = d_1$ as follows:

$$R(x = d_1) = \frac{Z(d_0) - Z_0}{Z(d_0) + Z_0} e^{i2k_0d} \quad (3)$$

where

$$Z_0 = \sqrt{\frac{\mu_0}{\epsilon_0}}, \quad Z(d_0) = \frac{\cos(kd)Z(d_1) + iZ \sin(kd)}{iY \sin(kd)Z(d_1) + \cos(kd)}, \quad Z(d_1) = \frac{E(d_1)}{H(d_1)} \quad (4)$$

Therefore, the reconstructed reflection coefficient, $R(x = d_1)$, contains only the reflection information of the target which was treated as the black box. Hence, with the full frequency band retrieved reflection coefficient, the information of the object, e.g., the distance, can be inversely obtained.

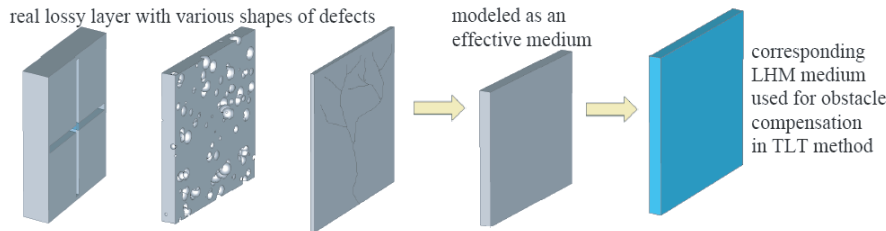


Figure 2. The procedure of modelling lossy layers when there are defects.

3. HOMOGENIZATION OF THE LOSSY LAYER WITH DEFECTS

The main challenge in the reality is that the lossy layer is inhomogeneous, which usually exists in real life, for example, cauterization, abrasion, scratch, perforation, and so on. These natural phenomena bring the obstacle layer various defects, which makes the imaging of the object a very challenging work. The inclusion of the defects has the same effect as the noise to the reflection coefficients measured by the receiver. If the lossy layer is perfectly homogeneous, we can get an ideal image of the target hidden behind the lossy wall using the reconstructed reflection coefficient obtained in the previous section. However, when the lossy layer contains defects with various kinds of geometries whose dimensions are much smaller than the working wavelengths, we can still model it as a homogeneous layer. The procedure of modeling is indicated in Fig. 2. We model the real lossy layers containing various shapes of air defects as homogeneous layers with effective parameters depending on the defects. Then in the process of compensating the reflection coefficient we use these modeled effective parameters to obtain the inverted matrix. Two kinds of lossy layers which are very typical in practice are investigated in this section.

3.1. Lossy Layer 1: Metallic Slab with FSS-like Defects

The first kind of lossy layer is a metal slab with different kinds of defects. A metal slab can be used as a shield to keep the object away from the

exposure of electromagnetic waves. However, sometimes the shield can be damaged by the outside force, yielding various kinds of slits or holes on it. These defects are usually smaller than the wavelength of the incident wave. In this subsection, we investigate such kind of defected metal layers. For simplicity, we consider the slots on the metal layer to be uniform and arranged in order. This configuration is very similar to the frequency selective surface (FSS). The frequency selective surface is a periodic metal surface which is basically an assembly of identical elements arranged in a one- or two-dimensional infinite array [15]. People are interested in the reflection or transmission of FSS at or around the resonance and make use of it, for instance, hybrid radomes, band-stop filters, dichroic sub-reflectors, etc. There are many types of FSS. In this subsection, we mainly discuss several examples as shown in Fig. 3, which the real defects are more inclined to be, despite some distortions in physical world.

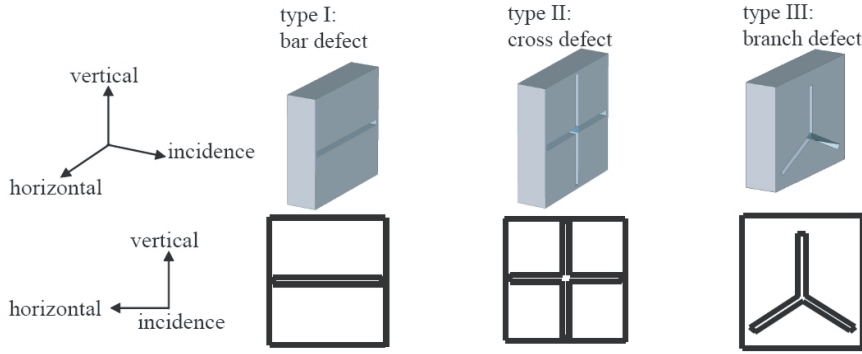


Figure 3. Unit cells for different types of defects in metal layer acting like FSS.

Unlike former researchers on FSS who concentrate only in the resonant region, we investigate the reflection and transmission property over a much wider frequency band for the sake of obtaining the effective parameters of metallic wall. For bulk metal materials, ideally they are described by a dielectric function of the same form as plasma media

$$\epsilon(\omega) = 1 - \frac{\omega_p^2}{\omega^2} \quad (5)$$

where ω_p is the plasma frequency, which is related to the electron density n , electron mass m_e , and electron charge e as

$$\omega_p^2 = \frac{ne^2}{\epsilon_0 m_e} \quad (6)$$

For most metals, the free electron density is at the order of 10^{22} cm^{-3} , and the plasma frequency ω_p is in the range of visible to ultraviolet (UV) wavelength. Eq. (5) is known as Drude model.

Pendry has proposed an effective medium theory that a thin-wire photonic structure behaves like a low density plasma of very heavy charged particles with a plasma frequency in the GHz range [16], and according to Eq. (6), presented an expression of plasma frequency for his structure model. Because the wire medium has a much smaller effective electron density but a much larger effective electron mass than those of the electrons in metallic film, it is evident that the plasma frequency of wires is much lower than that of the metal film, whose plasma frequency is usually located in the visible and near UV. The same principle can be applied to our model since the metallic film contain air defects which are able to lower the electron density. The key point is how we can estimate the position of effective ω_p in the Drude model.

One feasible method is based on the effective parameters retrieval algorithm [17], which is the determination process of effective permittivity and permeability of metamaterials from reflection and transmission coefficients. We use the simulation software (Microwave Studio) to simulate a plane wave normally incident onto the slab of the metallic layer with different types of defects, then we record the S_{11} and S_{21} data, from which the effective ϵ and μ at the whole frequency band can be inversely obtained. The retrieval effective permittivity and permeability for metallic layers with defects of the three prototypes (depicted in Fig. 3) are given in Fig. 4.

From Fig. 4, we can find the plasma frequencies of the metallic layer with different types of defects, which are all around 400 GHz. We also can see the retrieval results of the metal film with regularly arranged branch defects (Fig. 4(c)) are not so clear as the first two (Fig. 4(a) and Fig. 4(b)), but we still can roughly treat it as a dielectric material with a Drude model whose plasma frequency is up to over 400 GHz. The vibration below 400 GHz is due to the asymmetry along the horizontal and vertical line which causes some other resonance, but the main resonant effect owing to FSS is still dominant. We haven't show the results at very low frequencies because the absolute values of real part of ϵ_{eff} are too large, as well as the imaginary part. The retrieved permeability values have comparable small values (smaller than 0.1) and almost remain constant over the whole frequency band.

The effective parameters obtained from the retrieval method can be used as a comparison with some other analytical models, which is used to estimate the effective permittivity of the metallic films with FSS-like defects. As the retrieved results of effective permittivity

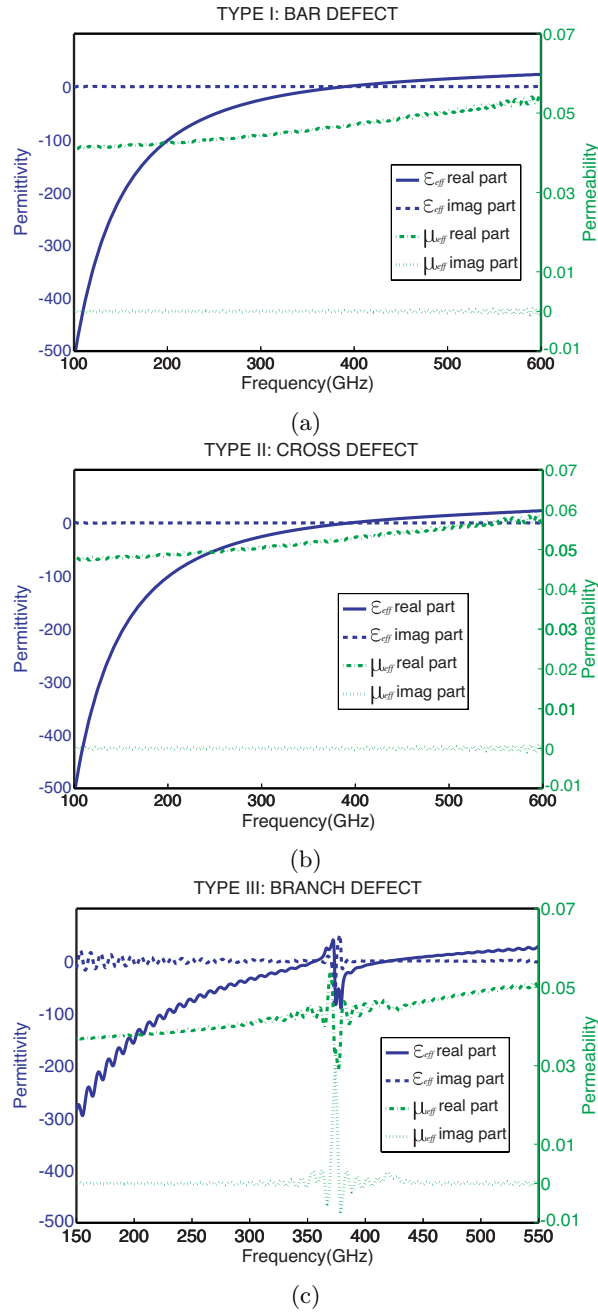


Figure 4. Retrieval results for the metal layers with different defects in Fig. 3.

and permeability for the three defected metallic layers are similar to each other, we consider them with the same proposed model. By comparing the values coming from the Drude model with retrieved ones, we find the aforementioned Drude model can be applied to fit the retrieved effective permittivity of the defected metal layer. The only improvement is that we include an additional coefficient ϵ for the original Drude model, which has the following form:

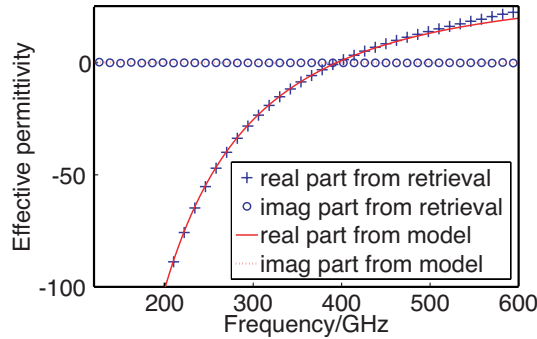


Figure 5. Comparison between retrieved effective permittivity and predicted values from our model for metal layer with type II (cross) defects.

$$\epsilon_{eff}(\omega) = \epsilon \left(1 - \frac{\omega_p^2}{\omega(\omega + i\gamma)} \right) \quad (7)$$

We take the cross defected layer (type II) as an example. In our simulation, an optimal ϵ value which is equal to 35 has been found, which is able to make the parameters from the model match best with the retrieval in the largest extend of the whole frequency, when the thickness of metal film is 0.1 mm ($\lambda_c/10$). Fig. 5 shows the comparison between the retrieved permittivity values and the predicted ones from Eq. (7) with parameters $\epsilon = 35$, $\omega_p = 394.0355$ GHz, and $\gamma = 0.1$ GHz. From the results, we can see that if the parameters in Eq. (7) are properly chosen, the curve predicted by our model agrees well with the retrieved results, except in very high frequency part. As the Drude model works well in most of the frequency band, we can use this model in the object imaging. In order to determine the three parameters (ϵ , ω_p , and γ) in the model, we can estimate the plasma frequency of the Drude model by retrieving the effective permittivity of the metal layer from its S_{11} and S_{21} parameters. If sometimes we cannot get the S -parameters for retrieval in reality, we can predict the plasma

frequency ω_p by other means, for example, we can roughly predict the effective ω_p by the dimensions of the patterns on the metal layer while the collision frequency γ and the coefficient ε can be determined based on the experience values.

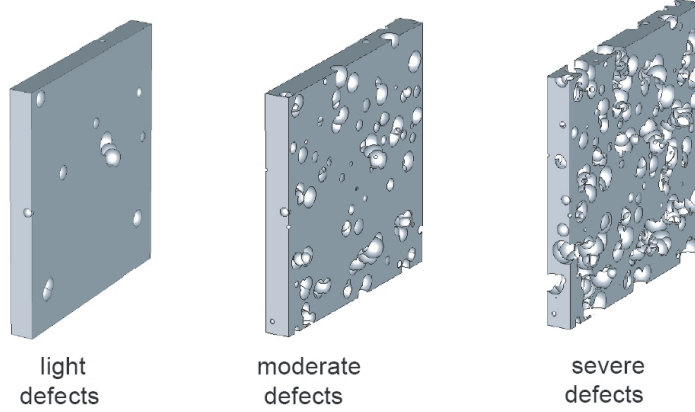


Figure 6. Lossy layers with different degrees of air bubble defects.

3.2. Lossy Layer 2: Plasma Slab with Air Bubbles Defects

In most cases, the lossy metallic “wall” is etched, corrupted, or perforated by small air inclusions. For these kinds of obstacles, we can model them as a plasma medium with air bubbles. The effective permittivity of the plasma layer will depend on the density of the defect. Fig. 6 shows different density of the air bubbles inside of the plasma layer. According to (Eq. (6)), when the air spheres are added to the plasma medium, the electrons in original plasma is diluted, which leads to a lower plasma frequency. We use the following equation to roughly predict the plasma frequency of the type of lossy layers:

$$\omega_p^2 = \frac{(1 - f_s)n_0e^2}{\varepsilon_0m_e} = (1 - f_s)\omega_{p0}^2 \quad (8)$$

where n_0 is the original electron density, ω_{p0} is the plasma frequency for the non-defected plasma medium, and f_s is fractional volume of air spheres. Eq. (8) tells how we predict the effective plasma frequency of the defected plasma layer when f_s is known.

Figure 7 shows the predicted ω_p (solid line) as a function of f_s by Eq. (8), which is compared with the retrieved effective plasma frequencies under different circumstances among large numbers of simulations. It should be noted that in the retrieval process, the air

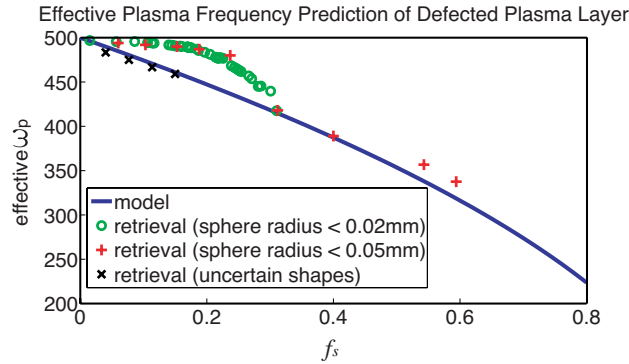


Figure 7. Predict effective plasma frequency for the defected plasma layer.

defects are randomly added into the plasma layer in the simulation and their sizes are also randomly extending from very tiny to a maximum value. For example, the plus marks in Fig. 7 stand for the air sphere defects whose upper limit radius is 0.05 mm, $\lambda_c/20$; and the circles are for average smaller spheres whose upper limit radius is 0.02 mm, $\lambda_c/20$. We also simulate several cases when the defects added into plasma layer are not sphere but with irregular shapes, and find the retrieved effective plasma frequencies (cross marks in Fig. 7) matches even better with the formula prediction.

4. APPLICATION AND RESULTS

In order to show the effect of our method in compensating the lossy layer with an active LHM slab, we compare the imaging results with the compensated reflection coefficients (compensated with proposed model and retrieval) and the original data. The inversion results for PEC target hidden behind a defected lossy wall are plotted in Figs. 8 and 9.

In Fig. 8, we consider a PEC target located at 25 mm away from sensor while an obstacle 10 mm away, which is a metallic film defected by a cross (type II in Fig. 3) with thickness 0.1 mm. The original reflection coefficient data, which we use to get the original target image, as the dot-dashed curve shows, is the S_{11} parameter (450~600 GHz) obtained in the simulation. When the retrieved ϵ_{eff} and μ_{eff} are used to compensate the reflection coefficient, the imaging result is illustrated by the dashed curve, from which we can see there is no significant improvement of the imaging quality. Using the parameter

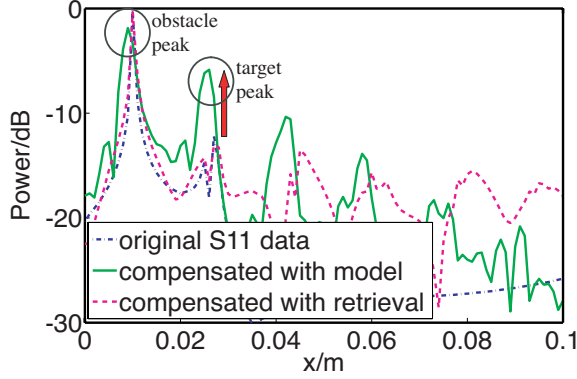
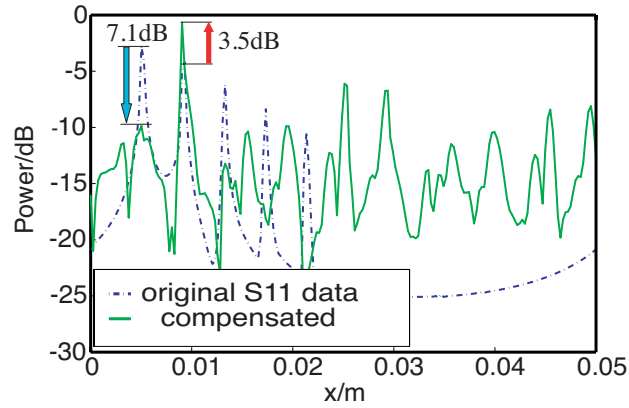


Figure 8. Imaging of PEC target behind a metal film with cross defects using partly frequency band 450~600 GHz.

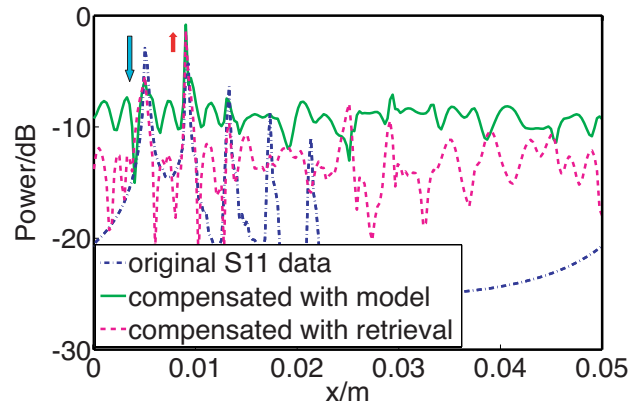
values from the proposed model (Eq. (7), $\epsilon = 35$, $\omega_p = 394.0355$ GHz, $\gamma = 0.1$ GHz), however, the solid curve shows the great enhancement at target peak while the obstacle peak gets more suppressed. So the effective parameter values from the Drude model works better than the retrieval method. This is because the retrieved effective parameter values contain noises during the retrieval procedure and the imaging procedure is an intrinsic inverse problem which is very sensitive to noise.

Figure 9 gives a more detailed example which shows how the incorrect estimates of the lossy layer's effective parameters affect the performance of our imaging method. In this case, the target is located at $x = 9$ mm and the obstacle is located at $x = 5$ mm. The obstacle layer is a plasma layer (background: $\omega_p = 500$ GHz, $\gamma = 10$ GHz) defected by different extents of air inclusions, with thickness 0.1 mm. Again, imaging results compensated with effective parameters from the Drude model (Eq. (8)) and with retrieved method are given in Figs. 9(b), 9(c), and 9(d).

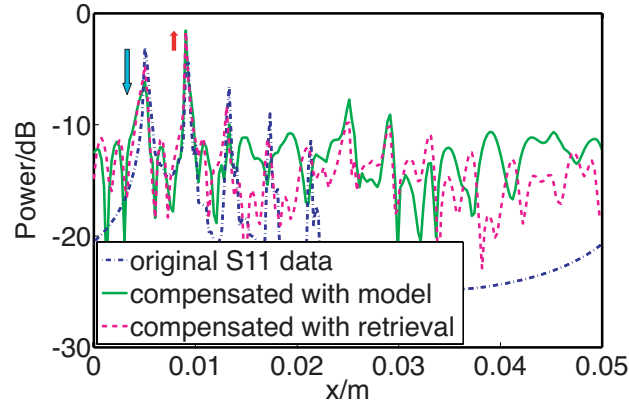
Figure 9(a) shows the imaging results for the plasma layer without defects ($f_s = 0$). The blue arrow pointing down marks the location where the obstacle peak is depressed and the red arrow pointing up shows the place where the target peak is enhanced. The imaging result after compensation [see solid curve] suppresses the obstacle peak by 7.1 dB and increase the target power 3.5 dB, compared with the one without compensation on the plasma layer [see dot-dashed curve]. Fig. 9(b) shows the imaging results for the plasma slab with a $f_s = 6\%$. We can see that the imaging quality by the Drude model (solid curve) is better than the retrieved method (dashed curve). The same result



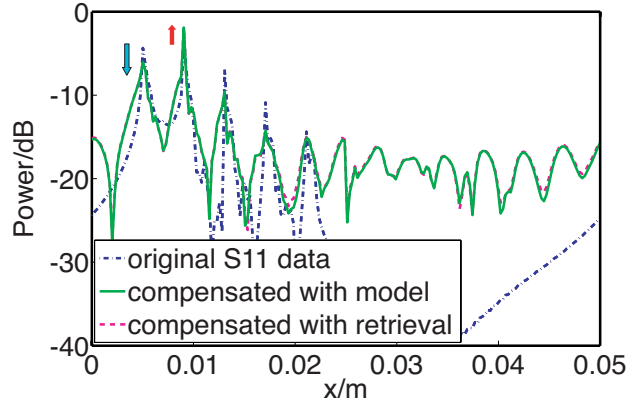
(a)



(b)



(c)



(d)

Figure 9. Imaging of PEC target behind the plasma layer with different f_s . The results are obtained from the whole frequency band 0~600 GHz simulated data.

happens when the air fractional volume percentage increases to 10.3% as shown in Fig. 9(c). However, the difference between the two results obtained by the two compensated images becomes smaller. When the air fractional volume is increased as much as 40%, we can hardly see any differences between the two sets of values because noise dominates the modelling and inversion process. However, compared with the one without compensation, the improvement of imaging quality using the compensation method can still be observed in Fig. 9(d).

5. CONCLUSION

To summarize, inverted matrix is used to cancel the effect of the lossy obstacle layer in the process of objects imaging. The imaging process using the Drude model are found to work better than that using retrieved parameters. The reason is due to the fact that the Drude model is less sensitive to the noise introduced in the numerical simulation than the retrieval method. Two kinds of lossy layer with different types of defects are investigated and have been used to test our inverted matrix compensation method. The performance of the method is obvious as long as we can get the right parameters of the obstacle. If we can model lossy layer damaged by different types of defects properly, this method of imaging through lossy layer is very helpful for us to find the right position of objects behind obstacle.

ACKNOWLEDGMENT

This work was supported in part by the Chinese Natural Science Foundation under Grant No. 60531020. X. X. Cheng would like to thank Dr. T. M. Grzegorzczuk for fruitful discussions.

REFERENCES

1. Mahfouz, M., A. Fathy, Y. Yang, E. E. Ali, and A. Badawi, "See-through-wall imaging using ultra wideband pulse systems," *Proceedings of the 34th Applied Imagery and Pattern Recognition Workshop (AIPR05)*, IEEE, Oct. 19–21, 2005.
2. Aryanfar, F. and K. Sarabandi, "Through wall imaging at microwave frequencies using space-time focusing," *Antennas and Propagation Society International Symposium, IEEE*, Vol. 3, 3063–3066, Jun. 20–25, 2004.
3. Guo, B., Y. Wang, J. Li, P. Stoica, and R. Wu, "Microwave imaging via adaptive beamforming methods for breast cancer detection," *J. of Electromagn. Waves and Appl.*, Vol. 20, No. 1, 53–63, 2006.
4. Chen, X., D. Liang, and K. Huang, "Microwave imaging 3-D buried objects using parallel genetic algorithm combined with FDTD technique," *J. of Electromagn. Waves and Appl.*, Vol. 20, No. 13, 1761–1774, 2006.
5. Oka, S., H. Togo, N. Kukutsu, and T. Nagatsuma, "Latest trends in millimeter-wave imaging technology," *Progress In Electromagnetics Research Letters*, Vol. 1, 197–204, 2008.
6. Ran, L., J. Huangfu, H. Chen, X. Zhang, K. Chen, T. M. Grzegorzczuk, and J. A. Kong, "Experimental study on several left-handed metamaterials," *Progress In Electromagnetics Research*, RIER 51, 249–279, 2005.
7. Shelby, R. A., D. R. Smith, and S. Schultz, "Experimental verification of a negative index of refraction," *Science*, Vol. 292, No. 6, 77, 2001.
8. Bilotti, F., A. Alu, N. Engheta, and L. Vegni, "Anomalous properties of scattering from cavities partially loaded with double-negative or single-negative metamaterials," *Progress In Electromagnetics Research*, PIER 51, 49–63, 2005.
9. Wu, B.-I., W. Wang, J. Pacheco, X. Chen, T. M. Grzegorzczuk, and J. A. Kong, "A study of using metamaterials as antenna substrate to enhance gain," *Progress In Electromagnetics Research*, PIER 51, 295–328, 2005.

10. Grzegorzczak, T. M. and J. A. Kong, "Review of left-handed metamaterials: Evolution from theoretical and numerical studies to potential applications," *J. of Electromagn. Waves and Appl.*, Vol. 20, No. 14, 2053–2064, 2006.
11. Guo, Y. and R. Xu, "Ultra-wideband power splitting/combining technique using zero-degree left-handed transmission lines," *J. of Electromagn. Waves and Appl.*, Vol. 21, No. 8, 1109–1118, 2007.
12. Li, Z. and T. J. Cui, "Novel waveguide directional couplers using left-handed materials," *J. of Electromagn. Waves and Appl.*, Vol. 21, No. 8, 1053–1062, 2007.
13. Abdalla, M. A. and Z. Hu, "On the study of left-handed coplanar waveguide coupler on Ferrite\(\mathbb{R}\)\Nsubstrate," *Progress In Electromagnetics Research Letters*, Vol. 1, 69–75, 2008.
14. Kong, J. A., *Electromagnetic Wave Theory*, EMW Publishing, Cambridge, Massachusetts, 2000.
15. Munk, B. A., *Frequency Selective Surfaces Theory and Design*, John Wiley & Sons, Inc., 2000.
16. Pendry, J. B., A. J. Holden, D. J. Robbins, and W. J. Stewart, "Low frequency plasmons in thin-wire structures," *J. Phys.: Condens. Matter*, Vol. 10, 4785–4809, 1998.
17. Chen, X., T. M. Grzegorzczak, B.-I. Wu, J. Pacheco Jr., and J. A. Kong, "Robust method to retrieve the constitutive effective parameters of metamaterials," *Physical Review E*, Vol. 70, No. 016608, 2004.